

Article

Composite Fe₃O₄-MXene-Carbon Nanotube Electrodes for Supercapacitors Prepared Using the New Colloidal Method

Wenyu Liang  and Igor Zhitomirsky *

Department of Materials Science and Engineering, McMaster University, Hamilton, ON L8S 4L7, Canada; liangw26@mcmaster.ca

* Correspondence: zhitom@mcmaster.ca

Abstract: MXenes, such as Ti₃C₂T_x, are promising materials for electrodes of supercapacitors (SCs). Colloidal techniques have potential for the fabrication of advanced Ti₃C₂T_x composites with high areal capacitance (C_S). This paper reports the fabrication of Ti₃C₂T_x-Fe₃O₄-multiwalled carbon nanotube (CNT) electrodes, which show C_S of 5.52 F cm⁻² in the negative potential range in 0.5 M Na₂SO₄ electrolyte. Good capacitive performance is achieved at a mass loading of 35 mg cm⁻² due to the use of Celestine blue (CB) as a co-dispersant for individual materials. The mechanisms of CB adsorption on Ti₃C₂T_x, Fe₃O₄, and CNTs and their electrostatic co-dispersion are discussed. The comparison of the capacitive behavior of Ti₃C₂T_x-Fe₃O₄-CNT electrodes with Ti₃C₂T_x-CNT and Fe₃O₄-CNT electrodes for the same active mass, electrode thickness and CNT content reveals a synergistic effect of the individual capacitive materials, which is observed due to the use of CB. The high C_S of Ti₃C₂T_x-Fe₃O₄-CNT composites makes them promising materials for application in negative electrodes of asymmetric SC devices.

Keywords: iron oxide; MXene; supercapacitor; electrode; dispersion; composite; carbon nanotube



Citation: Liang, W.; Zhitomirsky, I. Composite Fe₃O₄-MXene-Carbon Nanotube Electrodes for Supercapacitors Prepared Using the New Colloidal Method. *Materials* **2021**, *14*, 2930. <https://doi.org/10.3390/ma14112930>

Academic Editor: Suzy Surblé

Received: 30 April 2021

Accepted: 26 May 2021

Published: 29 May 2021

Publisher's Note: MDPI stays neutral with regard to jurisdictional claims in published maps and institutional affiliations.



Copyright: © 2021 by the authors. Licensee MDPI, Basel, Switzerland. This article is an open access article distributed under the terms and conditions of the Creative Commons Attribution (CC BY) license (<https://creativecommons.org/licenses/by/4.0/>).

1. Introduction

Ti₃C₂T_x belongs to the family of MXene-type materials, which are of great technological interest for applications in electrodes of SCs [1–3]. The interest in Ti₃C₂T_x is attributed to the high capacitance and low electrical resistivity of this material. The promising capacitive properties of Ti₃C₂T_x result from its high surface area and the redox active nature of surface functional groups. Enhanced capacitive properties were obtained for Ti₃C₂T_x composites, containing different conductive additives, such as graphene [4], acetylene black [5], and carbon black [6] and for nitrogen-doped Ti₃C₂T_x [7–9]. Moreover, advanced Ti₃C₂T_x composites were developed, containing other components, such as ZnO [10], MnO₂ [11], TiO₂ [12], and Mn₃O₄ [13]. Investigations revealed the stable cycling behavior of Ti₃C₂T_x composites [14–19].

High specific capacitance (C_m) normalized by active mass (AM) was reported for composite electrodes [9,12,14,20–28] with relatively low AMs, typically below 8 mg·cm⁻². The C_S of such electrodes was below 1 F·cm⁻². Capacitive properties of Ti₃C₂T_x composites were tested in various electrolytes, such as HCl [29], H₂SO₄ [27,30,31], KOH [12,32], KCl [33], K₂SO₄ [34], Na₂SO₄ [34], Li₂SO₄ [34], and other electrolytes [35,36]. Ti₃C₂T_x-based electrodes were utilized for the fabrication of symmetric SCs, containing two similar Ti₃C₂T_x-based electrodes, with maximum operation voltages in the range of 0.4–1.2 V [9,31,37,38].

The progress in applications of SC devices will depend on the ability to fabricate efficient electrodes and devices with high C_S, which can be achieved at high AM loadings. Another important benefit of high AM electrodes is their low ratio of the mass of electrochemically inactive components to the AMs. With the goal to increase energy–power characteristics, there is a growing trend in devices that operate in enlarged voltage windows. Of particular importance are environmentally friendly neutral electrolytes, such as

Na_2SO_4 , which facilitate the design of asymmetric aqueous cells with voltage windows above 1.2 V.

$\text{Ti}_3\text{C}_2\text{T}_x$ -based electrodes with AMs of $1\text{--}3\text{ mg cm}^{-2}$ were analyzed in Na_2SO_4 electrolyte [34,39,40] and relatively high C_m were obtained at such low AM loadings. Therefore, the development of electrodes with higher AMs can potentially result in high C_S . However, it is challenging [41] to achieve high C_S owing to the electrolyte diffusion limitations and high electrical resistance at high AMs. The increase in AM to the level of 20 mg cm^{-2} allowed the design of composites [42] with C_S of 1.087 F cm^{-2} at the galvanostatic charging conditions of 1 mA cm^{-2} and 0.783 F cm^{-2} at potential sweep conditions of 1 mV s^{-1} . Such electrodes [42] were utilized for symmetric $\text{Ti}_3\text{C}_2\text{T}_x$ SC.

The objective of this study was to form $\text{Fe}_3\text{O}_4\text{-Ti}_3\text{C}_2\text{T}_x\text{-CNT}$ electrodes for SCs. The use of CB as a co-dispersant allowed the fabrication of electrodes, which showed good electrochemical performance at AM of 35 mg cm^{-2} . CB allowed adsorption on individual materials and their dispersion due its polyaromatic structure, containing a chelating catechol ligand and electric charge. The experimental data of this investigation showed that C_S of 5.52 F cm^{-2} can be achieved in the negative potential range in $0.5\text{ M Na}_2\text{SO}_4$ electrolyte due to the use of advanced co-dispersant and a synergistic effect of the individual components.

2. Materials and Methods

Celestine blue (CB), $\text{FeCl}_3 \cdot 6\text{H}_2\text{O}$, $\text{FeCl}_2 \cdot 4\text{H}_2\text{O}$, NH_4OH , Na_2SO_4 , co-polymer of vinyl butyral, vinyl acetate and vinyl alcohol (PVBA, 65 kDa) were purchased from Millipore Sigma, Burlington, MA, USA. The diameter and length of CNT (multiwalled, Bayer Corp. Whippany, NJ, USA) were 13 nm and $1\text{--}2\text{ }\mu\text{m}$, respectively. $\text{Ti}_3\text{C}_2\text{T}_x$ was purchased from Laizhou Kai Kai Ceramic Materials Co., Ltd., Laizhou, China. Fe_3O_4 was prepared as described in by a chemical precipitation method [43] from solutions of FeCl_2 and FeCl_3 , containing dispersed CNT or co-dispersed CNT and $\text{Ti}_3\text{C}_2\text{T}_x$. In contrast to the previous investigation [43], pristine CNT were used. In this approach, CNT and $\text{Ti}_3\text{C}_2\text{T}_x$ were dispersed or co-dispersed using CB as a surfactant. For the fabrication of $\text{Fe}_3\text{O}_4\text{-CNT}$ electrodes, the synthesis of Fe_3O_4 was performed in the presence of CNT, dispersed using CB. For the fabrication of $\text{Ti}_3\text{C}_2\text{T}_x\text{-CNT}$ electrodes, $\text{Ti}_3\text{C}_2\text{T}_x$ was co-dispersed with CNT in water using CB as a co-dispersant. Active materials (AM) for $\text{Ti}_3\text{C}_2\text{T}_x\text{-Fe}_3\text{O}_4\text{-CNT}$ electrodes were prepared by precipitating Fe_3O_4 in the presence of co-dispersed $\text{Ti}_3\text{C}_2\text{T}_x$ and CNT. The amount of the CB dispersant in the suspension was 15% of the total mass of $\text{Ti}_3\text{C}_2\text{T}_x$, Fe_3O_4 and CNT. After filtration, obtained AM were washed with water and ethanol in order to remove non-adsorbed dispersant and dried in air. In order to analyze the effect of CB, AM for $\text{Ti}_3\text{C}_2\text{T}_x\text{-(Fe}_3\text{O}_4\text{-CNT)}$ electrodes were prepared by fabrication of $\text{Fe}_3\text{O}_4\text{-CNT}$ powder, as described above, and its mixing with $\text{Ti}_3\text{C}_2\text{T}_x$. The $\text{Ti}_3\text{C}_2\text{T}_x/\text{Fe}_3\text{O}_4$ mass ratio was 5:3 in the $\text{Ti}_3\text{C}_2\text{T}_x\text{-(Fe}_3\text{O}_4\text{-CNT)}$ and $\text{Ti}_3\text{C}_2\text{T}_x\text{-Fe}_3\text{O}_4\text{-CNT}$ electrodes. The mass ratio of CNT to the mass of active materials, such as Fe_3O_4 in $\text{Fe}_3\text{O}_4\text{-CNT}$, $\text{Ti}_3\text{C}_2\text{T}_x$ in $\text{Ti}_3\text{C}_2\text{T}_x\text{-CNT}$, Fe_3O_4 and $\text{Ti}_3\text{C}_2\text{T}_x$ (total) in $\text{Ti}_3\text{C}_2\text{T}_x\text{-(Fe}_3\text{O}_4\text{-CNT)}$ and $\text{Ti}_3\text{C}_2\text{T}_x\text{-Fe}_3\text{O}_4\text{-CNT}$ was 1:4.

Obtained powders were used for the fabrication of slurries in ethanol for the impregnation of commercial Ni foam current collectors (95% porosity, Vale, Rio de Janeiro, Brazil). The slurries contained dissolved PVBA binder. The mass of the binder was 3% of the total mass of the active material (AM). The total AM of impregnated material after drying was 35 mg cm^{-2} , which included 3% PVBA binder. All of the impregnated Ni foams were pressed using a calendaring machine in order to obtain a final electrode thickness of 0.38 mm.

Electrochemical impedance spectroscopy (EIS) and cyclic voltammetry (CV) studies were performed using a potentiostat (PARSTAT 2273, AMETEK, Berwyn, PA, USA). Galvanostatic charge discharge (GCD) was conducted using a Biologic AMP 300 potentiostat. The capacitive behavior of the electrodes was tested in an aqueous $0.5\text{ M Na}_2\text{SO}_4$ solution. Pt gauze was utilized as a counter electrode, and a saturated calomel electrode (SCE) was used as a reference. The area of the working electrode was 1 cm^2 . Capacitances C_S and C_m ,

normalized by the electrode area or mass of the active material, respectively, were obtained from the CV or GCD data, and complex C_S^* components (C_S' and C_S'') were calculated from the EIS testing results obtained at a signal of 5 mV, as described in [41]. JSM-7000F microscope (JEOL, Peabody, MA, USA) was used for SEM investigations.

3. Results and Discussion

Figure 1A,B shows SEM images of $Ti_3C_2T_x$ particles used in this investigation. The particles exhibit an accordion-like structure, which is beneficial for electrolyte access to the material. However, some small pores may not be accessible by the electrolyte. It is in this regard that the investigations of other pseudocapacitive materials did not show correlation between BET surface area and capacitance [44–47]. The SEM images of $Ti_3C_2T_x-Fe_3O_4-CNT$ composites (Figure 1C,D) show that $Ti_3C_2T_x$ particles were covered with Fe_3O_4 and CNT.

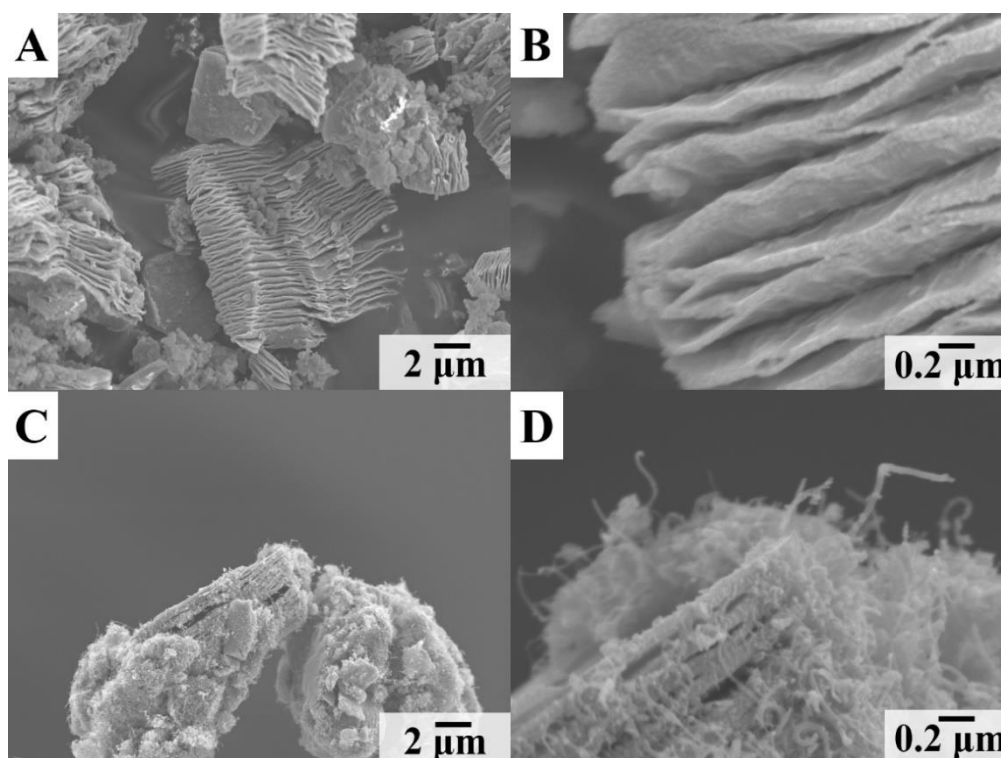


Figure 1. SEM images at different magnifications of (A,B) as-received $Ti_3C_2T_x$ and (C,D) $Ti_3C_2T_x-Fe_3O_4-CNT$.

$Ti_3C_2T_x$ particles were used for the fabrication of composite $Ti_3C_2T_x-Fe_3O_4-CNT$ electrodes. Pure $Ti_3C_2T_x-CNT$ and Fe_3O_4-CNT electrodes were also fabricated and tested for comparison. The X-ray diffraction patterns of the composite $Ti_3C_2T_x-CNT$, Fe_3O_4-CNT , and $Ti_3C_2T_x-Fe_3O_4-CNT$ materials presented in the Supplementary Information (Figure S1) show diffraction peaks of the individual components. All the electrodes contained 20% CNTs as conductive additives. In this investigation, CNTs were used as conductive additives for capacitive Fe_3O_4 [48–50] and $Ti_3C_2T_x$ [1–3] materials. Previous investigations highlighted the need for the fabrication of electrodes with high AMs and enhanced ratio of the AM to the mass of current collector and other passive components [41]. Commonly used so far are activated carbon (AC) commercial supercapacitors with high AM [41,51] of about $10 \text{ mg}\cdot\text{cm}^{-2}$. Another important parameter is electrode thickness [52]. It has been demonstrated that significant uncertainty in supercapacitor metrics stems from reporting gravimetric capacitance of thick electrodes with low packing density [51]. In such electrodes, empty space is filled by an electrolyte, thereby increasing the weight of the device without adding capacitance. However, such electrodes show enhanced AM normalized capacitance due to enhanced access of the electrolyte to the active materials [51]. Inves-

tigations showed that electrodes must be of comparable thickness for the comparison of their performance [53]. It is important to note that AC has a relatively low density and typical thickness of AC electrodes with active mass of $10 \text{ mg}\cdot\text{cm}^{-2}$ is about 0.6 mm [54]. In our investigation, the thickness of all the investigated electrodes was 0.38 mm and AM loading was $35 \text{ mg}\cdot\text{cm}^{-2}$. The higher AM of the fabricated electrodes, compared to that of AC electrodes, resulted from higher density of $\text{Ti}_3\text{C}_2\text{T}_x$ and Fe_3O_4 materials used in this investigation. The high AM loading was beneficial for increasing the ratio of AM - to the total mass, which includes not only AM, but also mass of current collectors, electrolyte and other components. The ability to achieve high capacitance using electrodes with high AM and low impedance is critical for the development of advanced electrodes.

In this investigation, CB was used as a dispersant for $\text{Ti}_3\text{C}_2\text{T}_x$, Fe_3O_4 and CNTs. CB has generated significant interest as an advanced dispersant for the fabrication of composites for supercapacitors and other applications [55–57]. Sedimentation tests showed good colloidal stability of the $\text{Ti}_3\text{C}_2\text{T}_x$, Fe_3O_4 and CNT suspensions, prepared using CB. It is important to note that the chemical structure of CB contains a catechol ligand, which facilitates CB adsorption on inorganic materials by complexation of metal atoms on the material surface [58]. Such interactions of CB with Ti atoms on the $\text{Ti}_3\text{C}_2\text{T}_x$ surface or Fe atoms on the Fe_3O_4 surface facilitated CB adsorption. The polyaromatic structure of CB allowed for its adsorption on CNTs and the adsorption mechanism of CB involved π - π interactions with side walls of CNTs [59]. The adsorbed cationic CB allowed for electrostatic dispersion of $\text{Ti}_3\text{C}_2\text{T}_x$, Fe_3O_4 and CNT and facilitated their enhanced mixing. Co-dispersion of $\text{Ti}_3\text{C}_2\text{T}_x$ with CNTs and Fe_3O_4 with CNTs allowed for good performance of $\text{Ti}_3\text{C}_2\text{T}_x$ -CNT and Fe_3O_4 -CNT electrodes at high AM loadings.

Figure 2 shows capacitive performances of $\text{Ti}_3\text{C}_2\text{T}_x$ -CNT and Fe_3O_4 -CNT electrodes. Cyclic voltammetry (CV) studies showed nearly rectangular shape CVs for $\text{Ti}_3\text{C}_2\text{T}_x$ -CNT electrodes and $C_S = 1.96 \text{ F}\cdot\text{cm}^{-2}$ at $2 \text{ mV}\cdot\text{s}^{-1}$. The obtained C_S was significantly higher than literature data for $\text{Ti}_3\text{C}_2\text{T}_x$ based electrodes, discussed in the Introduction. The capacitance retention at $100 \text{ mV}\cdot\text{s}^{-1}$ was 23.5%. Relatively high capacitances were also achieved using Fe_3O_4 -CNT electrodes. The highest $C_S = 4.42 \text{ F}\cdot\text{cm}^{-2}$ was attained at $2 \text{ mV}\cdot\text{s}^{-1}$. The use of CB as a co-dispersant allowed for higher capacitance of the Fe_3O_4 -CNT electrodes compared to the previous results [43] for the Fe_3O_4 -CNT electrodes, containing functionalized CNTs. The capacitance retention at $100 \text{ mV}\cdot\text{s}^{-1}$ was 14.9%. The capacitive properties of Fe_3O_4 -CNT composites resulted from the double layer charging mechanism of Fe_3O_4 and pseudocapacitive mechanism of Fe_3O_4 , attributed to $\text{Fe}^{2+}/\text{Fe}^{3+}$ redox couple [48–50].

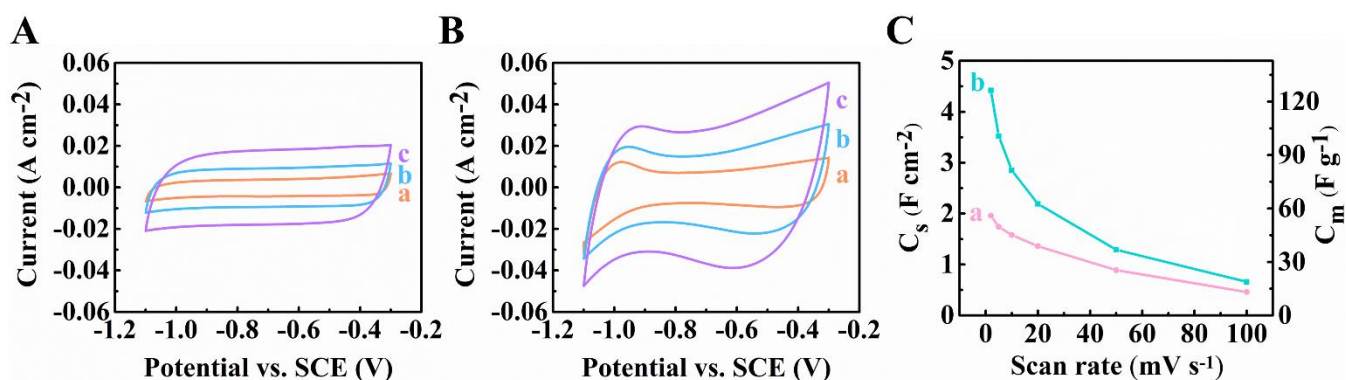


Figure 2. (A,B) Cyclic voltammetry data at (a) 2, (b) 5 and (c) $10 \text{ mV}\cdot\text{s}^{-1}$, (C) capacitances for ((A,C) (a)) $\text{Ti}_3\text{C}_2\text{T}_x$ -CNT and ((B,C) (b)) Fe_3O_4 -CNT electrodes.

Figure 3 shows EIS data for the $\text{Ti}_3\text{C}_2\text{T}_x$ -CNT and Fe_3O_4 -CNT electrodes. The Nyquist plot of complex impedance revealed lower resistance, $R = Z'$, compared to the literature data [42]. The low electrical resistance is an important factor controlling capacitive perfor-

mance of electrodes. The differential capacitance C_S' derived from the EIS data at 5 mV signal amplitude was inferior to the integral C_S calculated for potential span of 0.8 V. The discrepancy can be attributed to different parameters, such as charge–discharge time, electrode potential and limited accessibility of some redox sites at low voltages. The electrodes showed relatively high relaxation frequencies [60,61], corresponding to C_S'' maxima.

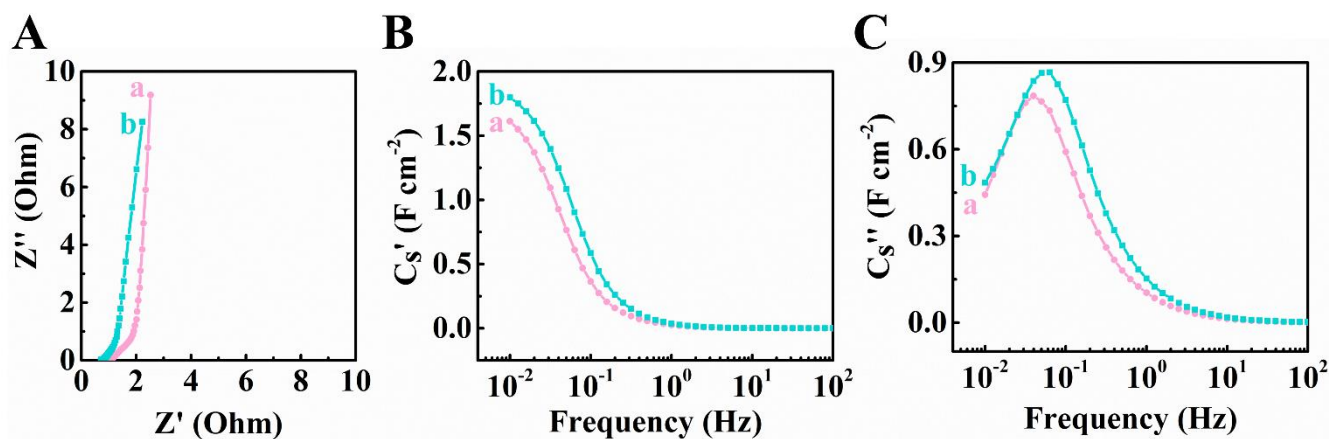


Figure 3. (A) Nyquist Z'' vs. Z' graph for EIS data, (B) C_S' and (C) C_S'' , derived from the EIS data for (a) $\text{Ti}_3\text{C}_2\text{T}_x$ -CNT and (b) Fe_3O_4 -CNT electrodes.

Figure 4A,B shows charge–discharge behavior of the $\text{Ti}_3\text{C}_2\text{T}_x$ -CNT and Fe_3O_4 -CNT electrodes. The electrodes showed nearly triangular symmetric GCD profile. The capacitances were calculated from the GCD data and are presented in Figure 4C. C_S reduced from 2.05 to 1.40 $\text{F}\cdot\text{cm}^{-2}$ and from 3.41 to 2.5 $\text{F}\cdot\text{cm}^{-2}$, for $\text{Ti}_3\text{C}_2\text{T}_x$ -CNT and Fe_3O_4 -CNT electrodes, respectively, in the current range 3–35 $\text{mA}\cdot\text{cm}^{-2}$. The GCD data showed good capacitance retention with increasing current density.

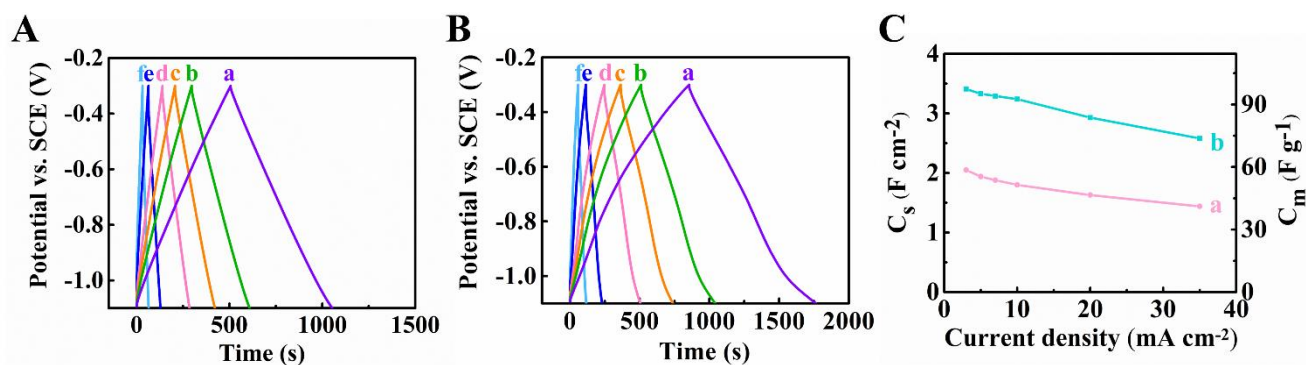


Figure 4. Galvanostatic charge–discharge curves of (A) $\text{Ti}_3\text{C}_2\text{T}_x$ -CNT, (B) Fe_3O_4 -CNT at (a) 3, (b) 5 (c) 7, (d) 10 (e) 20 and (f) 35 $\text{mA}\cdot\text{cm}^{-2}$, (C) capacitances derived from GCD tests for (a) $\text{Ti}_3\text{C}_2\text{T}_x$ -CNT and (b) Fe_3O_4 -CNT electrodes.

This investigation revealed a synergistic effect of $\text{Ti}_3\text{C}_2\text{T}_x$, CNT and Fe_3O_4 , which allowed for enhanced capacitance of the composite $\text{Ti}_3\text{C}_2\text{T}_x$ - Fe_3O_4 -CNT electrodes, compared to the capacitances of $\text{Ti}_3\text{C}_2\text{T}_x$ -CNT and Fe_3O_4 -CNT electrodes at the same AM, electrode thickness and CNT content. The use of CB as a dispersant was critical to achieve enhanced capacitance. The effect of CB is evident from the comparison of testing results for two composites, prepared at different experimental conditions, as was described in the Materials and Methods section. $\text{Ti}_3\text{C}_2\text{T}_x$ -(Fe_3O_4 -CNT) electrodes were prepared by precipitation of Fe_3O_4 in the presence of CNTs dispersed with CB, followed by washing drying and mixing with $\text{Ti}_3\text{C}_2\text{T}_x$. In contrast $\text{Ti}_3\text{C}_2\text{T}_x$ - Fe_3O_4 -CNT electrodes were prepared by precipitation of Fe_3O_4 in the presence of co-dispersed $\text{Ti}_3\text{C}_2\text{T}_x$ and CNTs.

CV testing results showed significantly larger CV areas for $\text{Ti}_3\text{C}_2\text{T}_\chi\text{-Fe}_3\text{O}_4\text{-CNT}$, compared to $\text{Ti}_3\text{C}_2\text{T}_\chi\text{-(Fe}_3\text{O}_4\text{-CNT)}$ electrodes (Figure 5A,B). This resulted in higher capacitance of the $\text{Ti}_3\text{C}_2\text{T}_\chi\text{-Fe}_3\text{O}_4\text{-CNT}$ and indicated the influence of CB dispersant used for the preparation of the composites on the properties of the electrodes. The highest capacitances of 5.52 and 3.90 $\text{F}\cdot\text{cm}^{-2}$ were obtained for $\text{Ti}_3\text{C}_2\text{T}_\chi\text{-Fe}_3\text{O}_4\text{-CNT}$ and $\text{Ti}_3\text{C}_2\text{T}_\chi\text{-(Fe}_3\text{O}_4\text{-CNT)}$ electrodes, respectively, at $2\text{ mV}\cdot\text{s}^{-1}$. In order to analyze the charge storage properties of the electrodes, a parameter b was calculated from the following equation [62,63].

$$i = av^b \quad (1)$$

where i is a current, v —scan rate and a is a parameter. Parameter b was found to be 0.68 for the $\text{Ti}_3\text{C}_2\text{T}_\chi\text{-Fe}_3\text{O}_4\text{-CNT}$ electrodes (Supplementary Information, Figure S2). It is known that $b = 1$ for purely double-layer capacitive mechanism and $b = 0.5$ for battery-type materials. The electrodes with $0.5 < b < 1$ combine capacitive and battery properties. According to [62], the battery-type charge storage mechanism is dominant for electrodes with $0.5 < b < 0.8$. Therefore, the $\text{Ti}_3\text{C}_2\text{T}_\chi\text{-Fe}_3\text{O}_4\text{-CNT}$ electrodes show mixed double-layer capacitive and battery-type properties with a dominant battery-type charge storage mechanism.

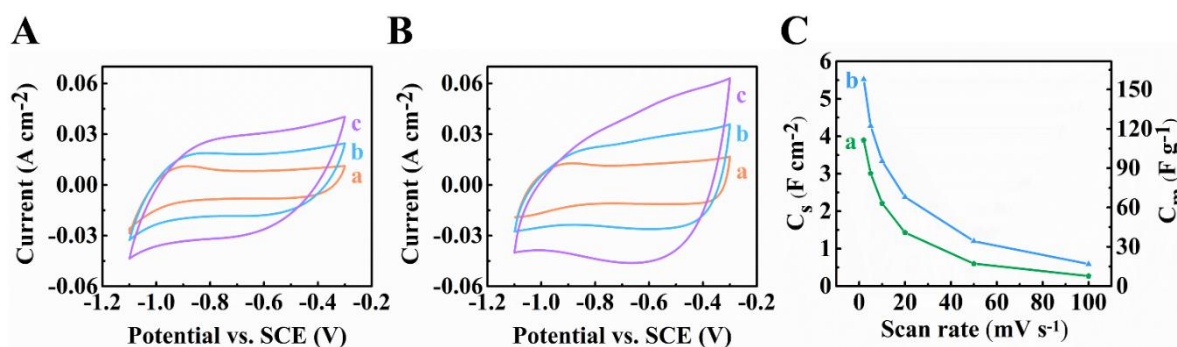


Figure 5. (A,B) Cyclic voltammetry data at (a) 2, (b) 5 and (c) 10 $\text{mV}\cdot\text{s}^{-1}$, (C) capacitances for ((A,C) (a) $\text{Ti}_3\text{C}_2\text{T}_\chi\text{-(Fe}_3\text{O}_4\text{-CNT)}$ and ((B,C) (b) $\text{Ti}_3\text{C}_2\text{T}_\chi\text{-Fe}_3\text{O}_4\text{-CNT}$ electrodes.

EIS studies (Figure 6) revealed lower resistance, higher capacitance and higher relaxation frequency of $\text{Ti}_3\text{C}_2\text{T}_\chi\text{-Fe}_3\text{O}_4\text{-CNT}$ electrodes, compared to $\text{Ti}_3\text{C}_2\text{T}_\chi\text{-(Fe}_3\text{O}_4\text{-CNT)}$ electrodes. GCD data showed nearly triangular symmetric charge–discharge curves, with longer charge and discharge times for $\text{Ti}_3\text{C}_2\text{T}_\chi\text{-Fe}_3\text{O}_4\text{-CNT}$ electrodes, compared to $\text{Ti}_3\text{C}_2\text{T}_\chi\text{-(Fe}_3\text{O}_4\text{-CNT)}$ at the same current densities (Figure 7A,B). The longer charge/discharge times indicated higher capacitances. The capacitances were calculated from the GCD data and presented in Figure 7C at different current densities. C_s reduced from 4.35 to 3.33 $\text{F}\cdot\text{cm}^{-2}$ and from 3.46 to 2.58 $\text{F}\cdot\text{cm}^{-2}$ for $\text{Ti}_3\text{C}_2\text{T}_\chi\text{-Fe}_3\text{O}_4\text{-CNT}$ and $\text{Ti}_3\text{C}_2\text{T}_\chi\text{-(Fe}_3\text{O}_4\text{-CNT)}$ composites, respectively, with current increase from 3 to 35 $\text{mA}\cdot\text{cm}^{-2}$.

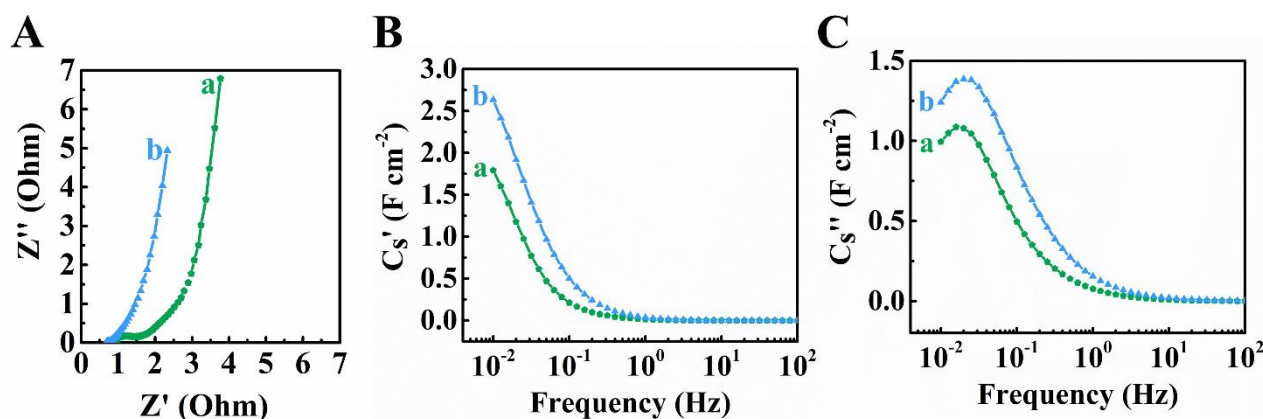


Figure 6. (A) Nyquist Z'' vs. Z' graph for EIS data, ((B,C)), (B) C_5' and (C) C_5'' , derived from the EIS data for (a) $Ti_3C_2T_x-(Fe_3O_4-CNT)$ and (b) $Ti_3C_2T_x-Fe_3O_4-CNT$ electrodes.

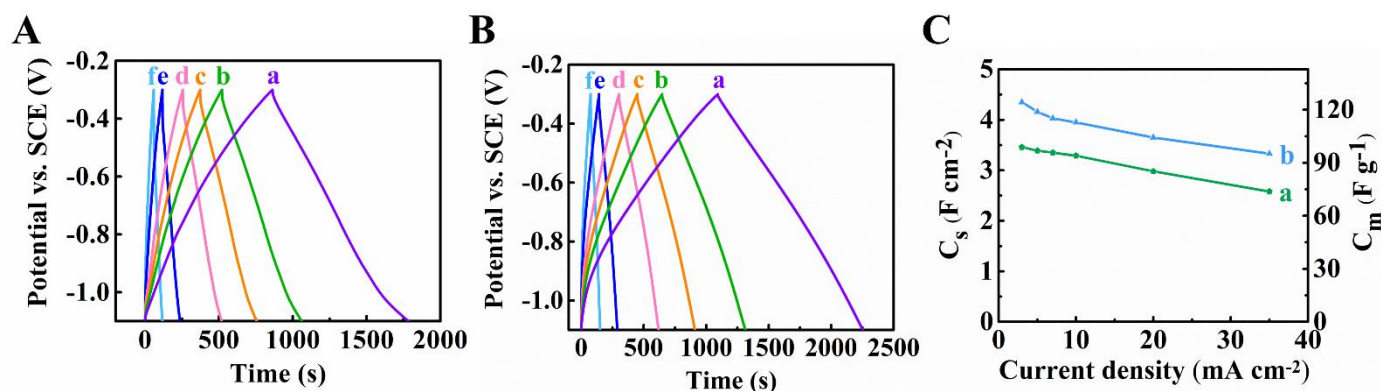


Figure 7. GCD curves for (A) $Ti_3C_2T_x-Fe_3O_4-CNT$, (B) $Ti_3C_2T_x-Fe_3O_4-CNT$ at (a) 3, (b) 5 (c) 7, (d) 10 (e) 20 and (f) 35 $mA\ cm^{-2}$, (C) capacitances versus current density, calculated from GCD data for (a) $Ti_3C_2T_x-(Fe_3O_4-CNT)$ and (b) $Ti_3C_2T_x-Fe_3O_4-CNT$.

The analysis of capacitances, measured using CV, EIS and GCD techniques showed that the capacitances of the $Ti_3C_2T_x-Fe_3O_4-CNT$ electrodes are higher than the capacitances of the $Ti_3C_2T_x-CNT$ and Fe_3O_4-CNT electrodes. Therefore, the experimental results of this work showed a synergistic effect of the individual capacitive materials. The comparison of the data for $Ti_3C_2T_x-Fe_3O_4-CNT$ and $Ti_3C_2T_x-(Fe_3O_4-CNT)$ electrodes and literature data of the previous investigations for $Ti_3C_2T_x$ [42] and Fe_3O_4 electrodes [43] showed the beneficial effect of co-dispersion of the individual components, which was achieved using CB as a dispersant. The ability to achieve high C_s of $5.52\ F\ cm^{-2}$ in the negative potential range in Na_2SO_4 is beneficial for the preparation of asymmetric SC. $Ti_3C_2T_x-Fe_3O_4-CNT$ electrodes showed relatively high C_s , compared to other anode materials [41]. The comparison with C_s for other $Ti_3C_2T_x$ -based electrodes in Na_2SO_4 electrolyte (Supplementary Information, Table S1) showed significant improvement in C_s . The capacitance of the negative electrodes is usually lower than that of positive electrodes. Advanced positive electrodes, based on MnO_2 , Mn_3O_4 , and $BiMn_2O_5$ have been developed with capacitance of about $5-8\ F\ cm^{-2}$ in the positive potential range [41]. Therefore, the capacitance of $Ti_3C_2T_x-Fe_3O_4-CNT$ s is comparable with capacitances of advanced positive electrodes. The $Ti_3C_2T_x-Fe_3O_4-CNT$ electrodes showed a slight C_s increase for the first 400 cycles and remained nearly constant after this initial increase (Figure 8). A similar increase was observed in the literature for other materials and was attributed to microstructure changes during initial cycling [64,65]. In contrast, the capacitance of the $Ti_3C_2T_x-CNT$ and Fe_3O_4-CNT electrodes decreased after cycling (Figure 8).

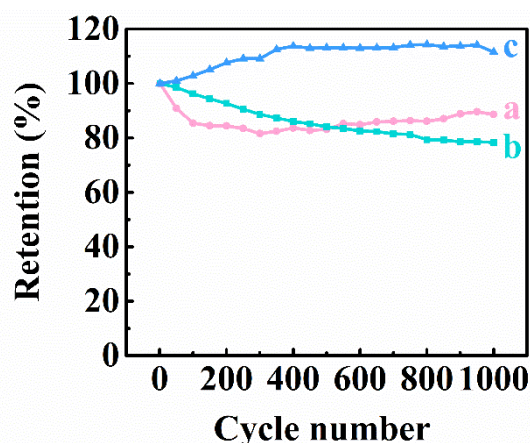


Figure 8. Capacitance retention for (a) Ti₃C₂T_x-CNT, (b) Fe₃O₄-CNT and (c) Ti₃C₂T_x-Fe₃O₄-CNT electrodes.

4. Conclusions

Ti₃C₂T_x-Fe₃O₄-CNT electrodes have been developed, which showed C_S of 5.52 F·cm⁻² in the negative potential range in 0.5 M Na₂SO₄ electrolyte. Such electrodes are promising for applications in asymmetric supercapacitor devices due to the high capacitance, which is comparable with the capacitance of advanced positive electrodes. The use of CB as an advanced co-dispersant allowed for the fabrication of Ti₃C₂T_x-Fe₃O₄-CNT electrodes, which showed good capacitive performance at high AM loadings. The comparison of capacitive behavior of Ti₃C₂T_x-Fe₃O₄-CNT electrodes with Ti₃C₂T_x-CNT and Fe₃O₄-CNT electrodes with the same AM, thickness and CNT content revealed a synergistic effect of the individual capacitive materials.

Supplementary Materials: The following are available online at <https://www.mdpi.com/article/10.3390/ma14112930/s1>. Figure S1: X-ray diffraction patterns of (a) Ti₃C₂T_x-CNT and (b) Fe₃O₄-CNT and (c) Ti₃C₂T_x-Fe₃O₄-CNT composites, Figure S2: Current (i) versus scan rate (ν) dependence in a logarithmic scale used for the calculation of parameter b for Ti₃C₂T_x-Fe₃O₄-CNT electrodes from the equation [1] $i = a\nu^b$, Table S1: Characteristics of Ti₃C₂T_x-based electrodes with high active mass in Na₂SO₄ electrolyte.

Author Contributions: Conceptualization, W.L. and I.Z.; methodology, W.L.; validation, W.L.; formal analysis, W.L.; investigation, W.L.; resources, I.Z.; data curation, W.L.; writing—original draft preparation, W.L. and I.Z.; writing—review and editing, W.L. and I.Z.; supervision, I.Z.; project administration, I.Z.; funding acquisition, I.Z. All authors have read and agreed to the published version of the manuscript.

Funding: This research was funded by the Natural Sciences and Engineering Research Council of Canada, grant number RGPIN-2018-04014.

Institutional Review Board Statement: Not Applicable.

Informed Consent Statement: Not Applicable.

Data Availability Statement: The data presented in this study are available in: “Composite Fe₃O₄-MXene-carbon nanotube electrodes for supercapacitors prepared by new colloidal method”.

Acknowledgments: SEM investigations were performed at the Canadian Centre for Electron Microscopy.

Conflicts of Interest: The authors declare no conflict of interest.

References

1. Anasori, B.; Lukatskaya, M.R.; Gogotsi, Y. 2D metal carbides and nitrides (MXenes) for energy storage. *Nat. Rev. Mater.* **2017**, *2*, 16098. [[CrossRef](#)]
2. Xu, S.; Wei, G.; Li, J.; Han, W.; Gogotsi, Y. Flexible MXene-graphene electrodes with high volumetric capacitance for integrated co-cathode energy conversion/storage devices. *J. Mater. Chem. A* **2017**, *5*, 17442–17451. [[CrossRef](#)]

3. Gogotsi, Y.; Anasori, B. The Rise of MXenes. *ACS Nano* **2019**, *13*, 8491–8494. [[CrossRef](#)]
4. Wang, K.; Zheng, B.; Mackinder, M.; Baule, N.; Qiao, H.; Jin, H.; Schuelke, T.; Fan, Q.H. Graphene wrapped MXene via plasma exfoliation for all-solid-state flexible supercapacitors. *Energy Storage Mater.* **2019**, *20*, 299–306. [[CrossRef](#)]
5. Guo, J.; Zhao, Y.; Jiang, N.; Liu, A.; Gao, L.; Li, Y.; Wang, H.; Ma, T. One-pot synthesis of 2D $\text{Ti}_3\text{C}_2/\text{Ni}_2\text{CO}_3(\text{OH})_2$ composite as electrode material with superior capacity and high stability for hybrid supercapacitor. *Electrochim. Acta* **2018**, *292*, 168–179. [[CrossRef](#)]
6. Gao, Y.; Wang, L.; Li, Z.; Zhang, Y.; Xing, B.; Zhang, C.; Zhou, A. Electrochemical performance of Ti_3C_2 supercapacitors in KOH electrolyte. *J. Adv. Ceram.* **2015**, *4*, 130–134. [[CrossRef](#)]
7. Tang, Y.; Zhu, J.; Wu, W.; Yang, C.; Lv, W.; Wang, F. Synthesis of Nitrogen-Doped Two-Dimensional Ti_3C_2 with Enhanced Electrochemical Performance. *J. Electrochem. Soc.* **2017**, *164*, A923–A929. [[CrossRef](#)]
8. Tian, Y.; Que, W.; Luo, Y.; Yang, C.; Yin, X.; Kong, L.B. Surface nitrogen-modified 2D titanium carbide (MXene) with high energy density for aqueous supercapacitor applications. *J. Mater. Chem. A* **2019**, *7*, 5416–5425. [[CrossRef](#)]
9. Wen, Y.; Rufford, T.E.; Chen, X.; Li, N.; Lyu, M.; Dai, L.; Wang, L. Nitrogen-doped $\text{Ti}_3\text{C}_2\text{T}_x$ MXene electrodes for high-performance supercapacitors. *Nano Energy* **2017**, *38*, 368–376. [[CrossRef](#)]
10. Wang, F.; Cao, M.; Qin, Y.; Zhu, J.; Wang, L.; Tang, Y. ZnO nanoparticle-decorated two-dimensional titanium carbide with enhanced supercapacitive performance. *RSC Adv.* **2016**, *6*, 88934–88942. [[CrossRef](#)]
11. Rakhi, R.B.; Ahmed, B.; Anjum, D.H.; Alshareef, H.N. Direct Chemical Synthesis of MnO_2 Nanowhiskers on Transition-Metal Carbide Surfaces for Supercapacitor Applications. *ACS Appl. Mater. Interfaces* **2016**, *8*, 18806–18814. [[CrossRef](#)] [[PubMed](#)]
12. Cao, M.; Wang, F.; Wang, L.; Wu, W.; Lv, W.; Zhu, J. Room Temperature Oxidation of Ti_3C_2 MXene for Supercapacitor Electrodes. *J. Electrochem. Soc.* **2017**, *164*, A3933–A3942. [[CrossRef](#)]
13. Oyedotun, K.O.; Momodu, D.Y.; Naguib, M.; Mirghni, A.A.; Masikhwa, T.M.; Khaleed, A.A.; Kebede, M.; Manyala, N. Electrochemical performance of two-dimensional $\text{Ti}_3\text{C}_2\text{-Mn}_3\text{O}_4$ nanocomposites and carbonized iron cations for hybrid supercapacitor electrodes. *Electrochim. Acta* **2019**, *301*, 487–499. [[CrossRef](#)]
14. Wang, H.; Zhang, J.; Wu, Y.; Huang, H.; Jiang, Q. Achieving high-rate capacitance of multi-layer titanium carbide (MXene) by liquid-phase exfoliation through Li-intercalation. *Electrochem. Commun.* **2017**, *81*, 48–51. [[CrossRef](#)]
15. Wu, W.; Niu, D.; Zhu, J.; Gao, Y.; Wei, D.; Zhao, C.; Wang, C.; Wang, F.; Wang, L.; Yang, L. Hierarchical architecture of $\text{Ti}_3\text{C}_2@\text{PDA}/\text{NiCo}_2\text{S}_4$ composite electrode as high-performance supercapacitors. *Ceram. Int.* **2019**, *45*, 16261–16269. [[CrossRef](#)]
16. Yang, C.; Que, W.; Tang, Y.; Tian, Y.; Yin, X. Nitrogen and Sulfur Co-Doped 2D Titanium Carbides for Enhanced Electrochemical Performance. *J. Electrochem. Soc.* **2017**, *164*, A1939–A1945. [[CrossRef](#)]
17. Yuan, W.; Cheng, L.; Zhang, B.; Wu, H. 2D- Ti_3C_2 as hard, conductive substrates to enhance the electrochemical performance of MnO_2 for supercapacitor applications. *Ceram. Int.* **2018**, *44*, 17539–17543. [[CrossRef](#)]
18. Zhang, C.; Wang, L.; Lei, W.; Wu, Y.; Li, C.; Khan, M.A.; Ouyang, Y.; Jiao, X.; Ye, H.; Mutahir, S.; et al. Achieving quick charge/discharge rate of 3.0 V s^{-1} by 2D titanium carbide (MXene) via N-doped carbon intercalation. *Mater. Lett.* **2019**, *234*, 21–25. [[CrossRef](#)]
19. Zhang, Y.; Yang, Z.; Zhang, B.; Li, J.; Lu, C.; Kong, L.; Liu, M. Self-assembly of secondary-formed multilayer La/e- Ti_3C_2 as high performance supercapacitive material with excellent cycle stability and high rate capability. *J. Alloys Compd.* **2020**, *835*, 155343. [[CrossRef](#)]
20. He, X.; Bi, T.; Zheng, X.; Zhu, W.; Jiang, J. Nickel cobalt sulfide nanoparticles grown on titanium carbide MXenes for high-performance supercapacitor. *Electrochim. Acta* **2020**, *332*, 135514. [[CrossRef](#)]
21. Hu, M.; Hu, T.; Li, Z.; Yang, Y.; Cheng, R.; Yang, J.; Cui, C.; Wang, X. Surface functional groups and interlayer water determine the electrochemical capacitance of $\text{Ti}_3\text{C}_2\text{T}_x$ MXene. *ACS Nano* **2018**, *12*, 3578–3586. [[CrossRef](#)] [[PubMed](#)]
22. Le, T.A.; Tran, N.Q.; Hong, Y.; Lee, H. Intertwined Titanium Carbide MXene within a 3D Tangled Polypyrrole Nanowires Matrix for Enhanced Supercapacitor Performances. *Chem. A Eur. J.* **2018**, *25*, 1037–1043. [[CrossRef](#)]
23. Li, Z.; Ma, C.; Wen, Y.; Wei, Z.; Xing, X.; Chu, J.; Yu, C.; Wang, K.; Wang, Z.-K. Highly conductive dodecaborate/MXene composites for high performance supercapacitors. *Nano Res.* **2019**, *13*, 196–202. [[CrossRef](#)]
24. Li, Y.; Deng, Y.; Zhang, J.; Han, Y.; Zhang, W.; Yang, X.; Zhang, X.; Jiang, W. Tunable energy storage capacity of two-dimensional $\text{Ti}_3\text{C}_2\text{T}_x$ modified by a facile two-step pillaring strategy for high performance supercapacitor electrodes. *Nanoscale* **2019**, *11*, 21981–21989. [[CrossRef](#)]
25. Lin, S.-Y.; Zhang, X. Two-dimensional titanium carbide electrode with large mass loading for supercapacitor. *J. Power Sources* **2015**, *294*, 354–359. [[CrossRef](#)]
26. Ramachandran, R.; Rajavel, K.; Xuan, W.; Lin, D.; Wang, F. Influence of $\text{Ti}_3\text{C}_2\text{T}_x$ (MXene) intercalation pseudocapacitance on electrochemical performance of Co-MOF binder-free electrode. *Ceram. Int.* **2018**, *44*, 14425–14431. [[CrossRef](#)]
27. Shen, L.; Zhou, X.; Zhang, X.; Zhang, Y.; Liu, Y.; Wang, W.; Si, W.; Dong, X. Carbon-intercalated $\text{Ti}_3\text{C}_2\text{T}_x$ MXene for high-performance electrochemical energy storage. *J. Mater. Chem. A* **2018**, *6*, 23513–23520. [[CrossRef](#)]
28. Yang, C.; Que, W.; Yin, X.; Tian, Y.; Yang, Y.; Que, M. Improved capacitance of nitrogen-doped delaminated two-dimensional titanium carbide by urea-assisted synthesis. *Electrochim. Acta* **2017**, *225*, 416–424. [[CrossRef](#)]
29. Lu, X.; Zhu, J.; Wu, W.; Zhang, B. Hierarchical architecture of $\text{PANI}@\text{TiO}_2/\text{Ti}_3\text{C}_2\text{T}_x$ ternary composite electrode for enhanced electrochemical performance. *Electrochim. Acta* **2017**, *228*, 282–289. [[CrossRef](#)]

30. Cao, J.; Han, Y.; Zheng, X.; Wang, Q. Preparation and electrochemical performance of modified $\text{Ti}_3\text{C}_2\text{T}_x$ /polypyrrole composites. *J. Appl. Polym. Sci.* **2019**, *136*, 47003. [[CrossRef](#)]
31. Jian, X.; He, M.; Chen, L.; Zhang, M.-M.; Li, R.; Gao, L.-J.; Fu, F.; Liang, Z.-H. Three-dimensional carambola-like MXene/polypyrrole composite produced by one-step co-electrodeposition method for electrochemical energy storage. *Electrochim. Acta* **2019**, *318*, 820–827. [[CrossRef](#)]
32. Li, X.; Zhu, J.; Wang, L.; Wu, W.; Fang, Y. In-situ growth of carbon nanotubes on two-dimensional titanium carbide for enhanced electrochemical performance. *Electrochim. Acta* **2017**, *258*, 291–301. [[CrossRef](#)]
33. Kim, K.; Okubo, M.; Yamada, A. Interfacial Dissociation of Contact-Ion-Pair on MXene Electrodes in Concentrated Aqueous Electrolytes. *J. Electrochem. Soc.* **2019**, *166*, A3739–A3744. [[CrossRef](#)]
34. Li, J.; Yuan, X.; Lin, C.; Yang, Y.; Xu, L.; Du, X.; Xie, J.; Lin, J.; Sun, J. Achieving High Pseudocapacitance of 2D Titanium Carbide (MXene) by Cation Intercalation and Surface Modification. *Adv. Energy Mater.* **2017**, *7*, 1602725. [[CrossRef](#)]
35. Luo, J.; Zhang, W.; Yuan, H.; Jin, C.; Zhang, L.; Huang, H.; Liang, C.; Xia, Y.; Zhang, J.; Gan, Y.; et al. Pillared Structure Design of MXene with Ultralarge Interlayer Spacing for High-Performance Lithium-Ion Capacitors. *ACS Nano* **2017**, *11*, 2459–2469. [[CrossRef](#)] [[PubMed](#)]
36. Shi, M.; Narayanasamy, M.; Yang, C.; Zhao, L.; Jiang, J.; Angaiah, S.; Yan, C. 3D interpenetrating assembly of partially oxidized MXene confined Mn–Fe bimetallic oxide for superior energy storage in ionic liquid. *Electrochim. Acta* **2020**, *334*, 135546. [[CrossRef](#)]
37. Li, H.; Chen, R.; Ali, M.; Lee, H.; Ko, M.J. In Situ Grown MWCNTs/MXenes Nanocomposites on Carbon Cloth for High-Performance Flexible Supercapacitors. *Adv. Funct. Mater.* **2020**, *30*, 2002739. [[CrossRef](#)]
38. Pan, Z.; Ji, X. Facile synthesis of nitrogen and oxygen co-doped $\text{C}@\text{Ti}_3\text{C}_2$ MXene for high performance symmetric supercapacitors. *J. Power Sources* **2019**, *439*, 227068. [[CrossRef](#)]
39. Wu, W.; Wei, D.; Zhu, J.; Niu, D.; Wang, F.; Wang, L.; Yang, L.; Yang, P.; Wang, C. Enhanced electrochemical performances of organ-like Ti_3C_2 MXenes/polypyrrole composites as supercapacitors electrode materials. *Ceram. Int.* **2019**, *45*, 7328–7337. [[CrossRef](#)]
40. Yang, B.; She, Y.; Zhang, C.; Kang, S.; Zhou, J.; Hu, W. Nitrogen Doped Intercalation $\text{TiO}_2/\text{TiN}/\text{Ti}_3\text{C}_2\text{T}_x$ Nanocomposite Electrodes with Enhanced Pseudocapacitance. *Nanomaterials* **2020**, *10*, 345. [[CrossRef](#)]
41. Chen, R.; Yu, M.; Sahu, R.P.; Puri, I.; Zhitomirsky, I. The Development of Pseudocapacitor Electrodes and Devices with High Active Mass Loading. *Adv. Energy Mater.* **2020**, *10*, 1903848. [[CrossRef](#)]
42. Guo, M.; Liu, C.; Zhang, Z.; Zhou, J.; Tang, Y.; Luo, S. Flexible $\text{Ti}_3\text{C}_2\text{T}_x@Al$ electrodes with Ultrahigh Areal Capacitance: In Situ Regulation of Interlayer Conductivity and Spacing. *Adv. Funct. Mater.* **2018**, *28*, 1803196. [[CrossRef](#)]
43. Nawwar, M.; Poon, R.; Chen, R.; Sahu, R.P.; Puri, I.K.; Zhitomirsky, I. High areal capacitance of Fe_3O_4 -decorated carbon nanotubes for supercapacitor electrodes. *Carbon Energy* **2019**, *1*, 124–133. [[CrossRef](#)]
44. Reddy, R.N.; Reddy, R.G. Sol–Gel MnO_2 as an electrode material for electrochemical capacitors. *J. Power Sources* **2003**, *124*, 330–337. [[CrossRef](#)]
45. Jeong, Y.U.; Manthiram, A. Nanocrystalline Manganese Oxides for Electrochemical Capacitors with Neutral Electrolytes. *J. Electrochem. Soc.* **2002**, *149*, A1419–A1422. [[CrossRef](#)]
46. Dong, W.; Rolison, D.R.; Dunn, B. Electrochemical Properties of High Surface Area Vanadium Oxide Aerogels. *Electrochem. Solid State Lett.* **1999**, *3*, 457–459. [[CrossRef](#)]
47. Dong, W.; Sakamoto, J.S.; Dunn, B. Electrochemical properties of vanadium oxide aerogels. *Sci. Technol. Adv. Mater.* **2003**, *4*, 3–11. [[CrossRef](#)]
48. Sinan, N.; Unur, E. Fe_3O_4 /carbon nanocomposite: Investigation of capacitive & magnetic properties for supercapacitor applications. *Mater. Chem. Phys.* **2016**, *183*, 571–579. [[CrossRef](#)]
49. Ghaly, H.A.; El-Deen, A.G.; Souaya, E.R.; Allam, N.K. Asymmetric supercapacitors based on 3D graphene-wrapped V_2O_5 nanospheres and $\text{Fe}_3\text{O}_4@3\text{D}$ graphene electrodes with high power and energy densities. *Electrochim. Acta* **2019**, *310*, 58–69. [[CrossRef](#)]
50. Nithya, V.D.; Arul, N.S. Progress and development of Fe_3O_4 electrodes for supercapacitors. *J. Mater. Chem. A* **2016**, *4*, 10767–10778. [[CrossRef](#)]
51. Gogotsi, Y.; Simon, P. True Performance Metrics in Electrochemical Energy Storage. *Science* **2011**, *334*, 917–918. [[CrossRef](#)]
52. Li, J.; Zhitomirsky, I. Cathodic electrophoretic deposition of manganese dioxide films. *Colloids Surf. A Physicochem. Eng. Asp.* **2009**, *348*, 248–253. [[CrossRef](#)]
53. Stoller, M.D.; Ruoff, R.S. Best practice methods for determining an electrode material's performance for ultracapacitors. *Energy Environ. Sci.* **2010**, *3*, 1294–1301. [[CrossRef](#)]
54. Chen, J.; Fang, K.; Chen, Q.; Xu, J.; Wong, C.-P. Integrated paper electrodes derived from cotton stalks for high-performance flexible supercapacitors. *Nano Energy* **2018**, *53*, 337–344. [[CrossRef](#)]
55. Liu, Y.; Zhitomirsky, I. Electrochemical supercapacitor based on multiferroic BiMn_2O_5 . *J. Power Sources* **2015**, *284*, 377–382. [[CrossRef](#)]
56. Liang, W.; Zhitomirsky, I. Zn-Fe Double Hydroxide-Carbon Nanotube Anodes for Asymmetric Supercapacitors. *Front. Mater.* **2020**, *7*, 137. [[CrossRef](#)]
57. Liu, Y.; Ata, M.S.; Shi, K.; Zhu, G.-Z.; Botton, G.A.; Zhitomirsky, I. Surface modification and cathodic electrophoretic deposition of ceramic materials and composites using celestine blue dye. *RSC Adv.* **2014**, *4*, 29652–29659. [[CrossRef](#)]

58. Ata, M.S.; Liu, Y.; Zhitomirsky, I. A review of new methods of surface chemical modification, dispersion and electrophoretic deposition of metal oxide particles. *RSC Adv.* **2014**, *4*, 22716–22732. [[CrossRef](#)]
59. Ata, M.S.; Poon, R.; Syed, A.M.; Milne, J.; Zhitomirsky, I. New developments in non-covalent surface modification, dispersion and electrophoretic deposition of carbon nanotubes. *Carbon* **2018**, *130*, 584–598. [[CrossRef](#)]
60. Zhu, Y.; Shi, K.; Zhitomirsky, I. Polypyrrole coated carbon nanotubes for supercapacitor devices with enhanced electrochemical performance. *J. Power Sources* **2014**, *268*, 233–239. [[CrossRef](#)]
61. Shi, K.; Zhitomirsky, I. Fabrication of Polypyrrole-Coated Carbon Nanotubes Using Oxidant–Surfactant Nanocrystals for Supercapacitor Electrodes with High Mass Loading and Enhanced Performance. *ACS Appl. Mater. Interfaces* **2013**, *5*, 13161–13170. [[CrossRef](#)]
62. Okhay, O.; Tkach, A. Graphene/Reduced Graphene Oxide-Carbon Nanotubes Composite Electrodes: From Capacitive to Battery-Type Behaviour. *Nanomaterials* **2021**, *11*, 1240. [[CrossRef](#)]
63. Gogotsi, Y.; Penner, R.M. Energy Storage in Nanomaterials—Capacitive, Pseudocapacitive, or Battery-like? *ACS Nano* **2018**, *12*, 2081–2083. [[CrossRef](#)] [[PubMed](#)]
64. Rorabeck, K.; Zhitomirsky, I. Application of Octanohydroxamic Acid for Salting out Liquid–Liquid Extraction of Materials for Energy Storage in Supercapacitors. *Molecules* **2021**, *26*, 296. [[CrossRef](#)] [[PubMed](#)]
65. Rorabeck, K.; Zhitomirsky, I. Salting-out aided dispersive extraction of Mn₃O₄ nanoparticles and carbon nanotubes for application in supercapacitors. *Colloids Surf. A Physicochem. Eng. Asp.* **2021**, *618*, 126451. [[CrossRef](#)]